AIP | Review of Scientific Instruments

Comparisons of a charge coupled device and a microchannel plate detector for Doppler spectroscopy

N. C. Hawkes

Citation: Rev. Sci. Instrum. **68**, 2051 (1997); doi: 10.1063/1.1148096
View online: http://dx.doi.org/10.1063/1.1148096
View Table of Contents: http://rsi.aip.org/resource/1/RSINAK/v68/i5
Published by the American Institute of Physics.

Related Articles

Quantum mechanical simulation of graphene photodetectors
J. Appl. Phys. 112, 084316 (2012)

Transient photoresponse and incident power dependence of high-efficiency germanium quantum dot photodetectors
J. Appl. Phys. 112, 083103 (2012)

Long-wave infrared nBn photodetectors based on InAs/InAsSb type-II superlattices
Appl. Phys. Lett. 101, 161114 (2012)

Infrared detectors based on semiconductor p-n junction of PbSe
J. Appl. Phys. 112, 086101 (2012)

Photocurrent spectroscopy of intersubband transitions in GaInAsN/(Al)GaAs asymmetric quantum well infrared photodetectors
J. Appl. Phys. 112, 084502 (2012)

Additional information on Rev. Sci. Instrum.

Journal Homepage: http://rsi.aip.org
Journal Information: http://rsi.aip.org/about/about_the_journal
Top downloads: http://rsi.aip.org/features/most_downloaded
Information for Authors: http://rsi.aip.org/authors

ADVERTISEMENT

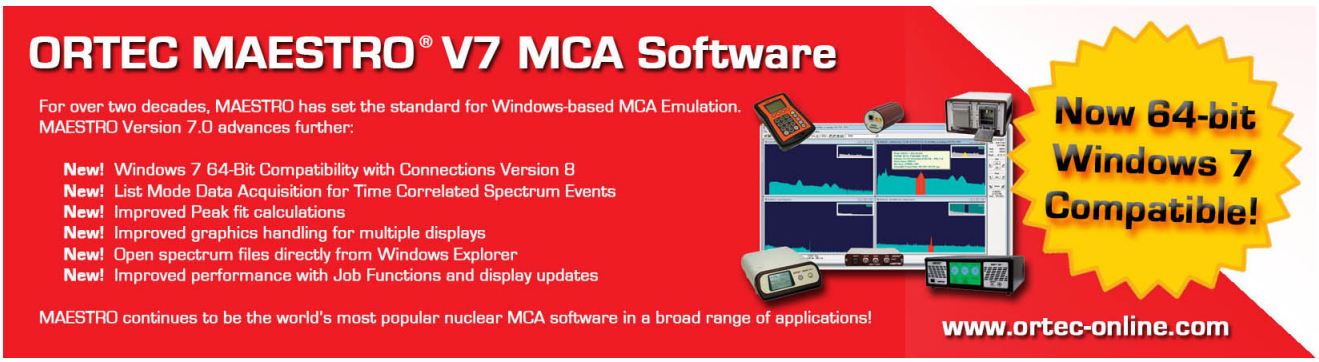

Comparisons of a charge coupled device and a microchannel plate detector for Doppler spectroscopy

N. C. Hawkes
UKAEA/Euratom Fusion Association, UKAEA, Fusion, Culham, Abingdon, Oxon OX14 3DB, United Kingdom

(Received 20 May 1996; accepted 20 January 1997)

Modern charge-coupled-device (CCD) detectors can achieve peak quantum efficiencies of 90%, compared with less than 10% for the photocathode of an electron multiplier. We report on laboratory tests of examples of these two detector technologies to evaluate their relative performance for precision Doppler spectroscopy of laboratory plasmas. The tests reveal that the accuracy of the Doppler width and shift measurements improves with the square root of the photoelectron flux, and thus as the square root of the detector quantum efficiency. An analytic estimate of the performance of these two types of detectors confirms the square root dependence on photoelectron flux but also highlights the importance of other noise sources that could be important under different conditions. The gain of the electron multiplier system can be reduced to the level of 10 photon-electrons per ADC count before there is any reduction in the accuracy of the estimation of fitted parameters. © *1997 American Institute of Physics.* [S0034-6748(97)00205-0]

I. INTRODUCTION

The quantum efficiency (QE) of modern back-thinned CCD detectors can now reach peak values of 90% (Ref. 1) (at 600 nm) while the QE of the photocathode used in microchannelplate (MCP) based image intensifiers is about 10% (at 450 nm). The improved QE of the CCD relative to the MCP image intensifier offers more detected photons for a given illumination intensity and therefore, in principle, provides better statistics for the fitting of spectral line shapes.

On the other hand, the enormous electron gain of a MCP allows counting of the separate photoevents with only modest noise performance of the associated amplifiers. With the CCD the readout noise of the device, although extremely low (typically five electrons), means that single photoevent detection is not possible. We report here the results of laboratory tests comparing these two types of detector with respect to the accuracy of measuring a spectral line position and width. The results of these tests are directly applicable to the measurement of ion velocities and temperatures from Doppler-shifted emission lines from a tokamak plasma.

II. EXPERIMENTAL ARRANGEMENT

For the measurements reported here, a McPherson spectrometer (model 209, 1.33 m) fitted with a 2400 l.mm^{-1} 120×140 mm grating (f/9) was used. The instrument has two exit ports and an insertable mirror, allowing the output spectrum to be directed to either of two detectors. The light source used for these measurements was a Perkin-Elmer type 303-606 samarium hollow cathode discharge lamp. The lamp is filled with neon and so emits strong neon lines in addition to samarium lines. The samarium emission line at 528.291 nm (Sm I) is close to the wavelength of the C VI $n = 8-7$ charge exchange line at 529.1 nm used in recent Doppler spectroscopy measurements.[2] The bright neon line at 630 nm is also very convenient for making alignment adjustments with the naked eye.

To obtain broadened spectral lines similar to those used in the Doppler measurements, the instrument was operated with a relatively wide entrance slit (140 μm). To produce line shapes similar to the Gaussian shapes obtained from thermally broadened plasma lines, the spectrometer was deliberately defocused by releasing the entrance slit from its mounting and withdrawing it about 4 mm from its normal position.

The spectrometer was fitted with a MCP-based image intensifier and diode array camera, as used for the Doppler measurements.[3] The alternate exit port was fitted with a commercial CCD camera for comparison.

A. MCP details

The MCP detector was a 40 mm dual MCP device with S-20 photocathode and P-20 output phosphor.[4] The photocathode quantum efficiency is shown in Fig. 1, taken from the manufacturer's data sheet, and is typical of such devices. The operating voltages were 4 kV on the phosphor (V_{ph}) and 1.4–1.6 kV at the photocathode (V_{pc}), with the biasing arrangement as shown in Fig. 2.

The output from the image intensifier was coupled by a coherent fiber optic bundle to a fast photodiode array camera.[5] This camera uses a Reticon S-series 1024 element photodiode array with pixels 25 μm×2.5 mm and has a readout rate of 1 μs per pixel at 12 bits resolution. The photodiodes in the Reticon recording the output of the MCP experience a thermally induced leakage current that contributes to the recorded signal, referred to as the dark current. This current varies from pixel to pixel and its contribution to the recorded signal increases as the integration time increases. There is also a component of signal due to the pick-up of clock line switching transients during the readout. Both these contributions can be subtracted from the recorded signals by reading out the array with no illumination. Therefore the readout of the diode array incorporated a sequence of 10 spectra that were taken after the data scans (referred to

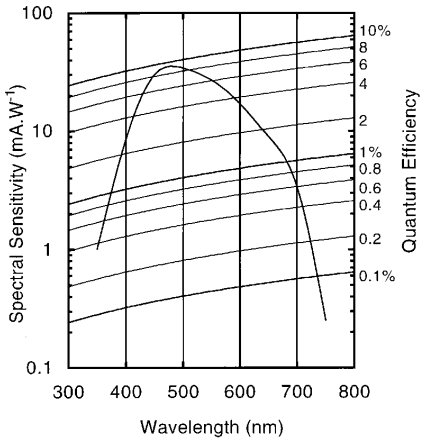

FIG. 1. Quantum efficiency curve for the photocathode of the MCP image intensifier (Photek Model MCP 240 EG, serial No. 2911122), from manufacturer's information.

as darkscans), with the input shutter on the spectrometer closed.

B. CCD details

The CCD used was an EEV chip, 22 μm 385×578 pixel, thinned and back-illuminated, with a phosphor coating to extend the short wavelength sensitivity below 500 nm. The technique of back-illumination of the CCD is used to avoid absorption of light in the electrode structure on the front of the chip and thus enhance the quantum efficiency compared to front-illuminated devices. The CCD was controlled and read out by a low noise camera system,[6] that also provided Peltier cooling to maintain the chip at 200 K to reduce charge build up from dark current. Figure 3 shows the quantum efficiency of the CCD.

A schematic of the layout of pixels on the chip is shown in Fig. 4. The upper (rows 291 to 578) and lower (rows 1 to 290) halves of the chip have separate clocking lines allowing the lower part to be used as an image store. In these measurements the pixels in the imaging area in the upper half of the chip were ''binned'' to form two elongated super-pixels 72 pixels high. The total area of each of these binned pixels was thus only 11% greater than the corresponding sensing area of the Reticon pixels. Using the lower half of the chip as an image store a minimum exposure time of 3 ms could be achieved. As with the MCP detector, readouts from the CCD with no illumination were subtracted from the spectral data to eliminate fixed background patterns.

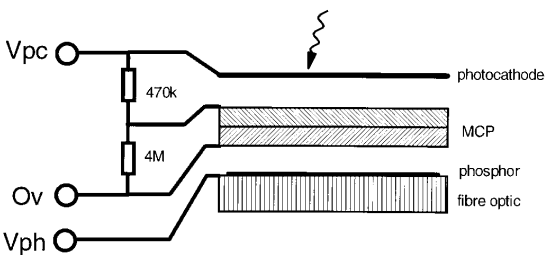

FIG. 2. Schematic of the components of the MCP image intensifier and the external bias resistor chain.

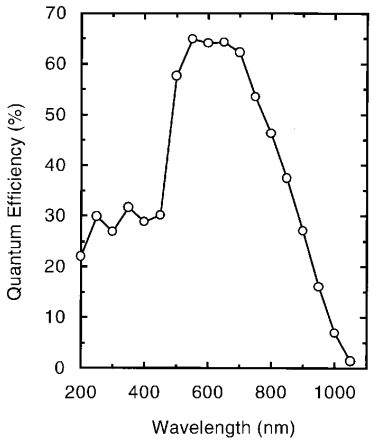

FIG. 3. Quantum efficiency of the CCD chip (taken from the manufacturer's data sheet).

III. LABORATORY MEASUREMENTS

A. Detector comparison

The initial comparison of the detector performance was performed at a range of integration times using the 528 nm Sm I line. The integration times of the Reticon measurements were made 11% shorter than the corresponding times for the CCD detector, to compensate for the different areas of the (binned) pixels in the two cases. The MCP data extend to shorter integration times than the CCD data since the Reticon detector was capable of faster readout. The MCP data were recorded with $V_{pc}=1.6$ kV and $V_{ph}=4$ kV, except for the longest (190 ms) integration times where V_{pc} had to be reduced (to 1.49 kV) to avoid saturation. (The separate effect of V_{pc} variations on the detector performance is discussed in Sec. III B.)

The data from the two detectors, recorded at various integration times, were least-squares fitted by a single Gaussian with a flat background using the Levenberg–Marquardt algorithm.[7] The fitting routine minimized the χ^2 parameter, with equal weights applied to all data points. The fitting was performed over 100 pixels of the CCD data or 88 pixels of

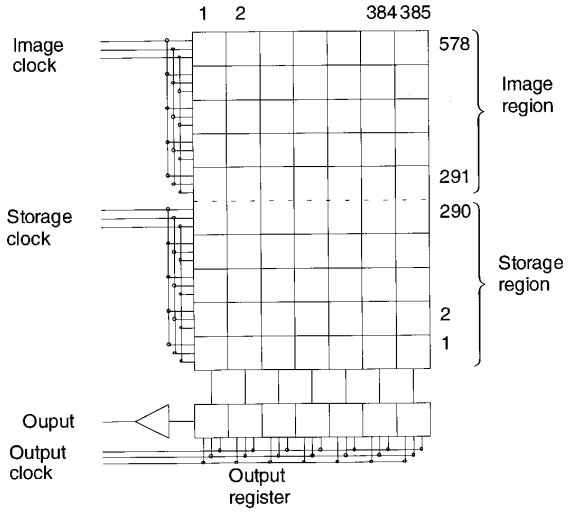

FIG. 4. Layout of pixels on the EEV CCD chip.

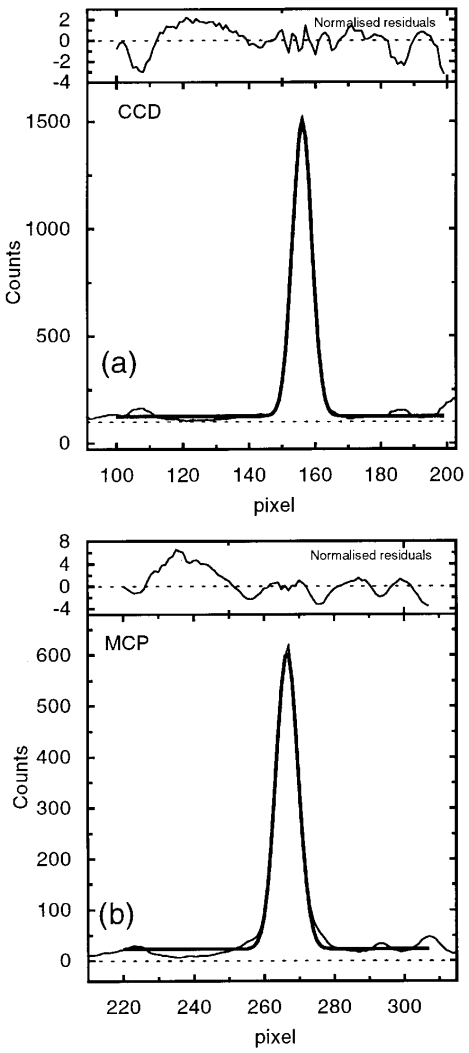

FIG. 5. Spectra from the CCD (a) and the MCP/Reticon (b) detectors at 12 and 10 ms integration time (respectively). Also shown are the Gaussians fitted to the spectral data.

the MCP data, corresponding to the same wavelength interval. Examples of the spectra from the two detectors, together with the fitted Gaussians, are shown in Fig. 5.

For each detector a sequence of spectra was recorded at each integration time and stored. For the CCD detector, 144 spectra were recorded (limited by the CCD chip storage area capacity) and for the MCP detector, 502 spectra and 10 dark scans (limited by the memory capacity of the CAMAC ADC used). Gaussian fitting was performed on these spectra and then the standard deviation of each parameter calculated from the list of fitted values. The standard deviations, σ, of the fitted parameters were used to judge the performance of the two detectors in respect of the width and position variation of the fitted Gaussians.

The σ values are listed for each detector as a function of exposure time in Table I and plotted in Fig. 6 against (exposure time)$^{-1/2}$. The curves exhibit an almost linear variation of σ with the inverse square root of exposure time, corresponding to the inverse square root of the total number of counts.

The best-fit linear curve through the MCP σ_{position} points has an intercept that is larger than that of the CCD σ_{position} points. The difference is small (and perhaps not statistically significant) but could be due to the higher dark current in the (uncooled) photodiodes of the MCP device. Such a difference would only become important at very long integration times, and necessarily very low photon fluxes, for example in astronomical imaging applications.

TABLE I. Table of standard deviations in the fitted width and position parameters from the least-squares fitting of a Gaussian profile to a sequence of spectra from the CCD and the MCP detector.

t_{CCD} (ms)	σ_{width} (pixels)	σ_{position} (pixels)	t_{MCP} (ms)	σ_{width} (pixels)	σ_{position} (pixels)
			1	0.162	0.144
4.3	0.036	0.032	4	0.089	0.080
8.5	0.026	0.023	8	0.067	0.060
13.8	0.018	0.017	14	0.051	0.048
24.1	0.012	0.011	24	0.041	0.036
53.1	0.012	0.010	48	0.027	0.024
189.5	0.006	0.004	190	0.016	0.015

B. MCP voltage scans

Data from the MCP detector were recorded at several different voltage settings (both V_{pc} and V_{ph}) at a constant integration time of 10 ms. The variations in peak count rate and σ for the width and position parameters are plotted in Fig. 7. There is very little variation in the σ values over the range of voltages explored, despite large changes to the intensifier gain, except at the lowest voltages, where the system response falls below 0.1 p-e count^{-1}. This behavior indicates that the primary photodetection process is the dominant contribution to the noise in these measurements (as opposed to readout noise), under normal detector operating conditions. The effect of different illumination levels is considered in the following section.

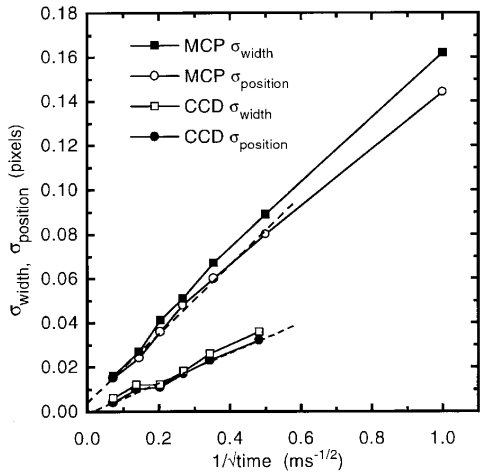

FIG. 6. Plot of standard deviation in fitted width and position parameters for the CCD and MCP detectors as a function of (exposure time)$^{-1/2}$. Linear regression line fits through the data are also shown.

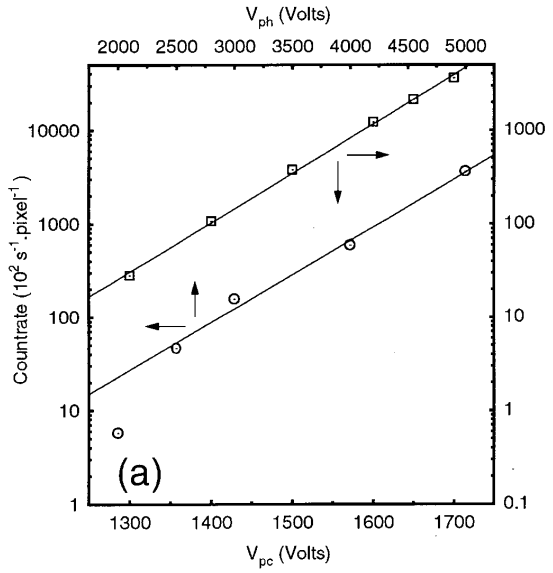

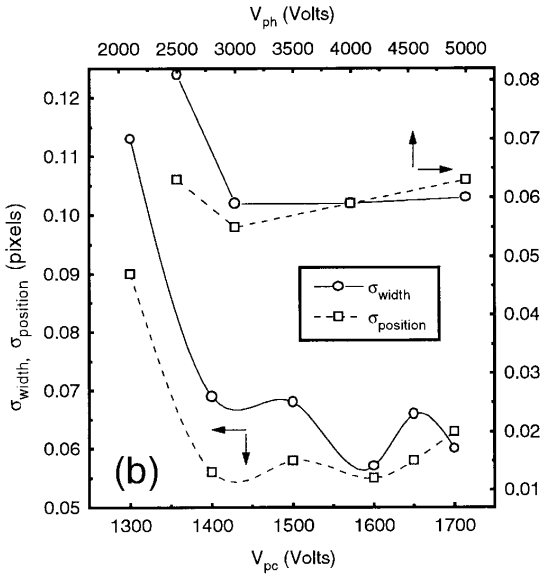

FIG. 7. Variation in: (a) detector gain (peak countrate) and (b) σ in the width and position parameters as a function of V_{pc} and V_{ph} for the MCP detector. No degradation in resolution is seen until the photocathode voltage is reduced below 1400 V or the phosphor voltage below 4 kV, representing in each case a gain reduction of more than a factor of 20 compared to the maximum voltages, $V_{pc} = 1700$ V and $V_{ph} = 5000$ V. (While either V_{pc} and V_{ph} was altered, the other voltage was maintained at maximum.)

C. Effect of intensity variations

The effect of different intensities on the accuracy of fitted position and width was studied by recording data from several spectral lines over a wide wavelength range with each detector. Since the detector gains were not varied the intensities measured in each case were proportional to the photoelectron count rate. The exposure time data of Table I were taken with the same detector gains and are therefore directly comparable with the data at different wavelengths and so are also included in this data set. In Fig. 8 the σ values for each detector are plotted against (peak height)$^{-1/2}$, expressed in photoelectrons using the QE curves of Figs. 1 and 3.

Plotting the data against the photoelectron rate, rather than simply the exposure time (as in Fig. 6) the data from the CCD and the MCP detectors lie along the same curve, linear at high count rates (low σ). Since the data include measurements at various wavelengths and hence different quantum efficiencies, this shows that the critical parameter affecting the fitting σ is the photoelectron flux, rather than the input photon flux. The figure also shows two model calculations of the fitting σ at different photoelectron flux rates, based on data concerning the readout noise of the two detector systems. The basis of these models is discussed in Sec. V.

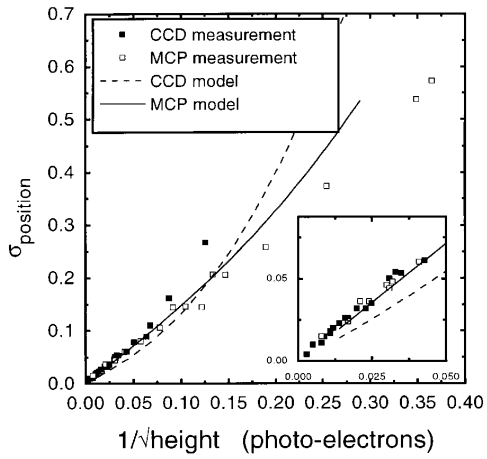

FIG. 8. Plot of σ_{position} against $1/\sqrt{\text{height}}$ for a range of intensities and exposure times with the height expressed in photoelectrons. Solid and dashed lines are the result of a model prediction taking into account the readout noise associated with each detector (Sec. V).

The σ data obtained from the two detectors are plotted in Fig. 9 as a function of wavelength. Since the intensities of the lines selected varied somewhat, the σ values are compared by plotting their ratio between the two detectors at each wavelength. The intensities of the lamp lines used in these measurements correspond to the linear portion of the data in Fig. 8 (except at 350 nm), and therefore the ratio of σ between the two detectors is expected to follow $\sqrt{\text{QE}}$ (shown as a broken line in the figure), as is in fact found.

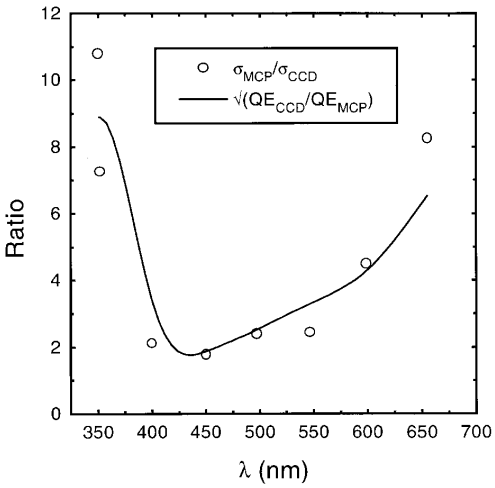

FIG. 9. Ratio of σ_{position} plotted against wavelength together with the square root of the QE ratio between the two detectors.

TABLE II. Data for the dependence of σ_{position} on the width of the line. The table includes data using a narrow entrance slit, a slightly defocused entrance slit, and a grossly defocused auxiliary slit. Various weak lamp lines were used. The fourth column shows the results of an expression [Eq. (1)] fitted to the σ_{position} data.

Height (counts)	Width (pixels)	σ_{position} (pixels)	σ_{fit} (pixels)
218.8	31.4	0.426	0.405
149.2	4.27	0.118	0.124
48.3	29.5	0.878	0.825
51.2	33.5	0.785	0.875
1098	4.27	0.048	0.046

D. Linewidth variation

To estimate the effect of linewidth variation on the fitting accuracy, the spectrometer was further defocused. This was accomplished by opening the main entrance slit fully (to about 6 mm) and placing an auxiliary slit 60 mm in front of the spectrometer slit. This produced a line image that was generally trapezoidal but could be made roughly triangular by adjustment of the auxiliary slitwidth. The half-width of the triangular line in this configuration was about 40 pixels, comparable with the typical Gaussian linewidths obtained during tokamak measurements. A lamp line was selected, at 418.4 nm, that gave a similar intensity to the C VI 529 nm line from the tokamak and measurements of the line were made with the MCP detector. The spectrometer main slit was then closed to 150 μm which had the effect of narrowing the line while keeping its peak height constant.

The results of these measurements, including others with the defocused slit and weaker lines, are presented in Table II. From these data, and the assumption that σ_{position} has an inverse square root dependence on height and a power law dependence on width, an empirical fit to the position uncertainty can be extracted:

$$\sigma_{\text{fit}} = 0.5596\ \text{height}^{-0.5}\ \text{width}^{0.6876}. \quad (1)$$

This expression is evaluated in the fourth column of Table II and gives reasonable agreement with the measured σ_{position}.

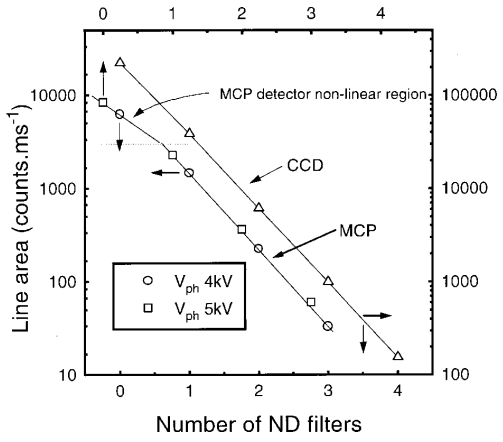

FIG. 10. Line area plotted against neutral density for the MCP detector at two different voltages, and for the CCD detector. The CCD detector is linear over the entire range, while the MCP detector shows nonlinearity in response at high signal levels. The dependence of the nonlinearity on phosphor voltage indicates that the nonlinearity arises in the phosphor response.

The dependence of σ_{position} on the inverse square root of the height can again be seen in the data of the table by comparing rows with similar width parameter, either 30 or 4 pixels.

E. Linearity checks

For this test a strong lamp line ($\lambda = 640$ nm) was selected and various neutral density filters were inserted in front of the entrance slit. The MCP detector was operated with $V_{pc} = 1.6$ kV, $V_{ph} = 4$ kV, and a 1 ms exposure time. The resulting curve of line area against total filter density in Fig. 10 shows a deviation from linearity at the highest intensity.

To check that the source of the nonlinearity was not in the photodiodes or signal processing electronics, the exposure with no filter was repeated at an integration time of 3 ms, increasing the size of the diode stored charge. The measured area was exactly three times that recorded at 1 ms, to within one standard deviation (i.e., to within 1%), showing that the nonlinearity was not occurring in the charge storage or readout processes. To verify that the nonlinearity was occurring within the MCP/phosphor, and not the photocathode, the sequence of exposures was repeated at a higher phosphor operating voltage ($V_{ph} = 5$ kV). This second curve is also plotted in Fig. 10, but translated in the x direction by an amount equivalent to the gain change due to the change in V_{ph} [derived from Fig. 7(a)]. Here the nonlinearity was found to be more severe at the higher countrates. From the two curves it is apparent that the nonlinearity sets in at a particular count rate and becomes more severe as the count rate increases, even when the illumination intensity remains the same. Since the increase in count rate was achieved by increasing the electron gain at the phosphor the nonlinearity must be (at least in part) due to the phosphor response.

The nonlinearity sets in at a count rate of 3000 ms^{-1}, thus care has to be taken during measurements to keep below this level, if necessary by adjusting the detector voltages. The results of Fig. 7(b) showed that a considerable reduction in detector voltages was possible before there was any significant impact on the estimation of line shape parameters.

The signal levels measured with no attenuation were much greater than the maximum signals recorded during tokamak measurements, so the nonlinearity seen with the MCP detector should not present a problem during normal operation in tokamak experiments. A third curve is plotted in Fig. 10, that of the line area measured as a function of neutral density for the CCD detector. This curve shows that the CCD is exceptionally linear over the entire dynamic range explored.

F. Instrument function

The instrument functions of the combination of detector and spectrometer were measured for each detector with the spectrometer fully focused. A narrow (50 μm) entrance slit was used, with 632.8 nm light from a HeNe laser (attenuated by scattering from a white screen to avoid the risk of damaging the MCP photocathode). The resulting instrument functions are shown in Fig. 11 and show that the CCD and spectrometer combined have an instrument function with line

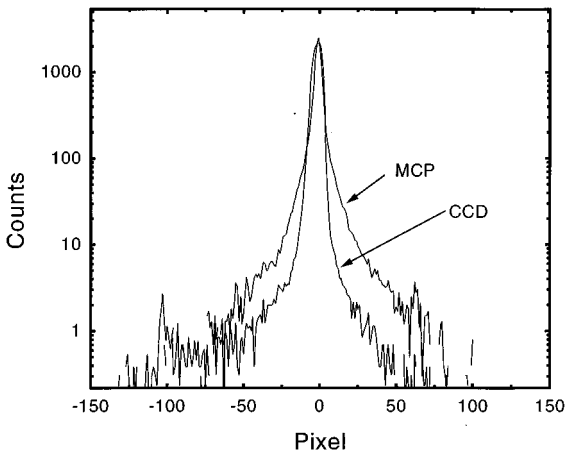

FIG. 11. The instrument functions of the combination of detector and spectrometer measured using the CCD and the MCP detectors, at the HeNe 632.8 nm laser wavelength.

wings that (at 20 pixels away from the line center) are lower by at least a factor of three compared to the MCP-based detector. The smaller pixel size of the CCD detector makes the line profile effectively narrower still compared to the MCP detector.

IV. TOKAMAK MEASUREMENTS

Final tests were carried out using charge exchange excited emission from a tokamak plasma at Culham (JET), exploiting the reaction between neutral heating beams and fully ionized carbon:

$$C^{6+} + H^0 \rightarrow C^{5+}* + H^+.$$

The Doppler broadened emission from the excited C^{5+} ions is Gaussian of typically 40 pixels full width. It was necessary to validate the results of the laboratory studies with a true Gaussian source, although the use of plasma emission imposes other difficulties, chiefly, a time varying Doppler shift due to plasma mass motion.

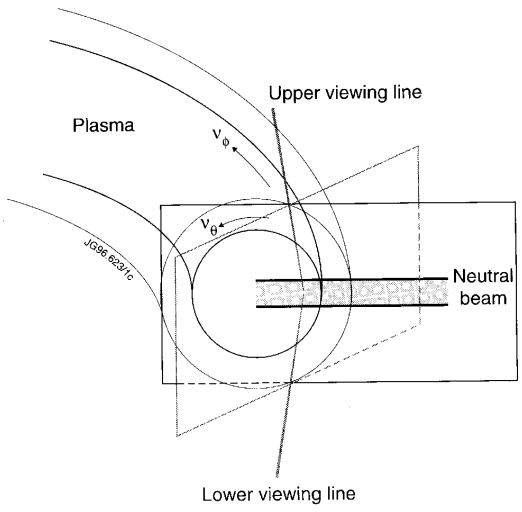

FIG. 12. Geometry of viewing observation on the JET tokamak: The two viewing lines used in these measurements lie in a plane angled with respect to the poloidal plane. They are also tilted away from the vertical direction within this plane. This geometry allows resolution of the measured Doppler shifts into toroidal, v_ϕ, and poloidal, v_θ, flows. Of these, v_θ is expected to be small, allowing this quantity to be used as a test of the position fitting accuracy.

The apparatus used in these measurements was the same as that used for the laboratory tests except for the addition of a second spectrometer in the input path of the model 209. This spectrometer serves to band limit the light entering the model 209 and allows multiple slits to be used along the dispersion direction.[8] Two of the fibers from the multichord collecting optics were connected to adjacent entrance slits of the spectrometer. Vertically opposing views were used allowing the Doppler shifts of the emission light to be resolved into poloidal (vertical) and toroidal (horizontal) flow velocities (Fig. 12). Since the poloidal velocities are very low, this resolved component could be regarded as constant and hence used to obtain a statistical measurement of the fitted line center positions, for comparison with the lamp measurements.

The image region of the CCD was organized as a single binned area, the binned images were stored on the chip and read out after the plasma pulse. In this way 288 pairs of spectra could be recorded. The timing of the storage of spectra was such that the data acquisition window was 8 s long, enough to cover the entire charge exchange pulse of 5 s with some overlap into the noncharge exchange periods.

In this comparison, data were recorded from two successive JET discharges that are similar (except for the duration of the charge exchange pulse). For the second discharge the MCP detector was used and the results from the two detectors compared.

A. Results and analysis

The data from each detector were treated in a similar fashion. In each case background subtraction and pixel gain calibration were applied and then the data least squares fitted with a single Gaussian line profile. The raw fitted parameters were then converted to physical parameters of ion temperature, toroidal, and poloidal flow velocities. For the background subtraction in the case of the CCD detector another acquisition sequence was triggered with no light falling on the detector. From these data, 100 scans were averaged to give a background signal representing the no-light response of each (binned) CCD pixel. For the MCP detector 10 background scans were automatically recorded before plasma initiation at the start of each JET shot. To calibrate the different pixel sensitivities (incorporating the response curve of the combined spectrometers) spectra were recorded with a tungsten lamp illuminating the entrance slits. These spectra were normalized such that when divided into the plasma data they corrected for small variations in pixel-to-pixel responses, but left the overall amplitude the same. The integration time for the CCD measurements was 27.9 ms, that of the MCP measurements 28.7 ms.

The results of the measurements with the two detectors are shown in Figs. 13 and 14, with the Doppler shifts for the two views resolved into toroidal, v_ϕ, and poloidal, v_θ, plasma velocities. The figures include the time history of the brightness of the deuterium $n=3-2$ transition (D_α) re-

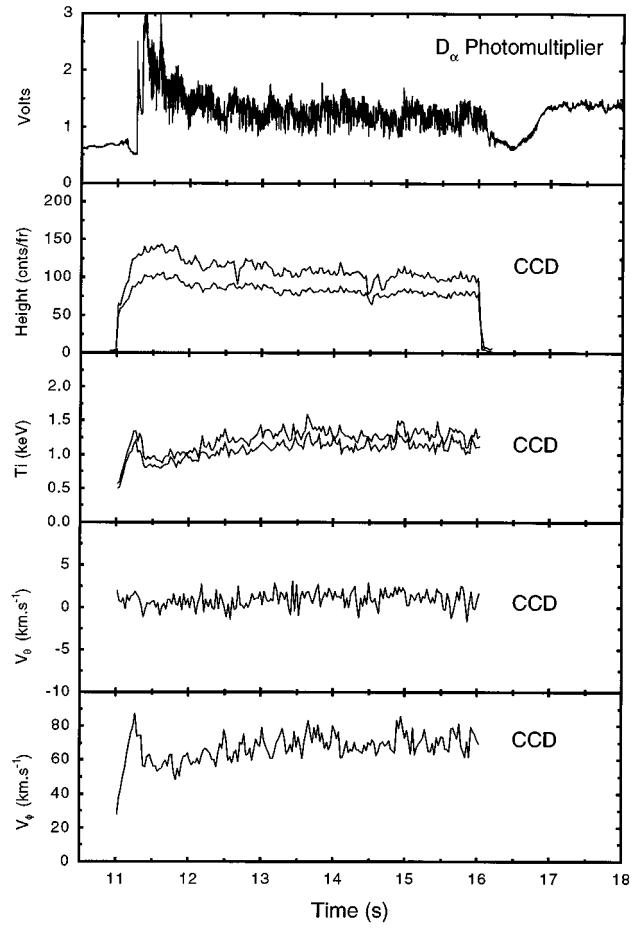

FIG. 13. Derived ion parameters from a tokamak shot using a CCD detector and two opposed edge views. Two traces are shown in the height and temperature plots, one from each view, while the velocity plots have only a single value, composed of the vector resolved components of the ion flows. The D_α emission, recorded with a separate photomultiplier system, is indicative of changes in plasma confinement and density.

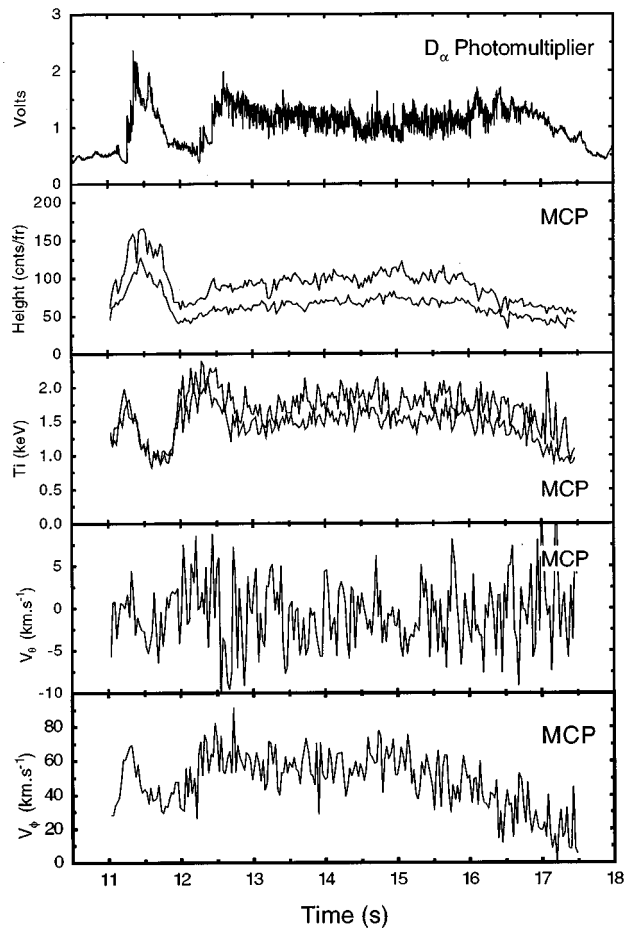

FIG. 14. Derived ion parameters from a tokamak shot using the MCP detector.

corded separately with a filter and photomultiplier. This time trace shows intensity fluctuations that depend upon various plasma conditions including heating, density, and confinement mode. The zeros of the v_ϕ and v_θ velocities are arbitrary since the unshifted line positions have not been referred to a standard wavelength. The lower noise in the measurement of v_θ with the CCD detector (compared with the same quantity measured with the MCP detector) is immediately apparent. Variations (of about 15 km s^{-1}) can be seen in the toroidal flow, v_ϕ, between 12.5 and 13.5 s with a period of 4 Hz, correlated with fluctuations in D_α and related to the deliberate oscillation of the plasma boundary. A significant reduction in the noise level of the ion temperature measurements is also evident in the data from the CCD detector.

B. Comparison of noise levels with laboratory measurements

To quantify the differences in the scatter of the measurements with the two detectors it is necessary to compare the poloidal flow signals. All the other parameters are changing with time during the two discharges while the poloidal flow speed is expected (and indeed appears) to be small. This parameter is derived from a difference in the Doppler shift of light from the two opposing views of the plasma, there being an equal Doppler shift on each single chord due to the component of toroidal rotation along their lines of sight.

The fitted height and width parameters from the CCD data are used according to the scaling of Eq. (1), to obtain a prediction of the standard deviation of the fitted Gaussian position. The scaling is expressed in terms of photoelectrons and therefore the raw height parameter is corrected for the sensitivity of the CCD—5.05 photoelectrons per ADC count (manufacturer's data) at the gain setting used in the measurements. Since the poloidal flow velocity is obtained from a difference of two fitted positions the errors in the two parameters are added in quadrature and converted to a velocity deviation, $\sigma_{v_\theta} = 1.65$ km s^{-1}. This is to be compared to the measured deviation in the poloidal flow velocity of 0.892 km s^{-1} between 12.88 and 15.33 s, showing reasonable agreement.

The analysis of the MCP data is similar, except that here the fitted height is adjusted for the different operating conditions (a phosphor voltage of 4 kV as opposed to 5 kV in Sec. III A, giving a gain change of 2.073, from the data of Fig. 7) and the different pixel size of the MCP detector is accounted for in the conversion from pixels to velocity. This analysis yields a predicted value for the MCP data of $\sigma_{v_\theta} = 6.96$ km s^{-1} compared to the measured value of 3.95 km s^{-1} obtained between 13.5 and 17.5 s.

In each case the measured deviation is a little over half the predicted deviation, based on the laboratory scaling. The difference reflects the difficulty of obtaining an adequate scaling [Eq. (1)] for the linewidth based on data from a low temperature laboratory source. The inverse square root dependence on line height correctly predicts the lower deviation observed with the CCD detector.

V. DISCUSSION

The important result that emerges from the data in the preceding sections is that the precision to which a wavelength can be measured varies as the square root of the number of photoelectrons detected. This empirical result can be understood from a consideration of the estimated variance of the fitted position.

For a nonlinear least-squares fit of a function to experimental data the variance of a single fitted parameter, α, can be written,[9]

$$\sigma_\alpha^2=\frac{\sum \frac{1}{\sigma_i^2}\left(\frac{\partial y_i}{\partial \alpha}\right)^2}{\left\{\sum \frac{1}{\sigma_i^2}\left[\left(\frac{\partial y_i}{\partial \alpha}\right)^2-(s_i-y_i)\left(\frac{\partial^2 y_i}{\partial \alpha^2}\right)\right]\right\}^2}, \tag{2}$$

where y_i is the fitted function evaluated at the ith point, α is the parameter whose variance, σ_α^2, is to be estimated, s_i is the number of photoelectrons detected in the ith channel and σ_i^2 the variance of the ith data point. Taking the fitting function to be a Gaussian;

$$y_i=Ae^{-(x_i-p)^2/w^2} \tag{3}$$

with A the peak amplitude, x_i the pixel number, and p and w the position and width parameters (ignoring the constant background parameter for simplicity). Assuming Poisson statistics for the photodetection process, $\sigma_i^2=y_i$, the estimated variance on the position becomes,

$$\sigma_{\text{position}}^2=\frac{\sum \frac{1}{y_i}\left[\frac{2(x_i-p)}{w^2}y_i\right]^2}{\left\{\sum \frac{1}{y_i}\left[\left(\frac{2(x_i-p)}{w^2}y_i\right)^2-(s_i-y_i)\left(-\frac{2}{w^2}y_i+\frac{4(x_i-p)^2}{w^4}y_i\right)\right]\right\}^2}. \tag{4}$$

In this expression, only the terms y_i depend on the amplitude of the fitted Gaussian, A. Assuming that the term s_i also varies like A then an overall dependence of $\sigma_{\text{position}} \propto 1/\sqrt{A}$ is found, as observed in the measurements. A similar analysis for σ_{width} also yields a dependence of $\sigma_{\text{width}} \propto 1/\sqrt{A}$. No such simple dependence of σ_{position} or σ_{width} on the fitted linewidth, w, can be extracted due to the nonlinear dependence of y_i on w.

The assumption of Poisson statistics is a simplification since there is a contribution to the detector noise from the statistics of the photoelectron detection process. This noise affects the performance of a device, its performance in the presence of this noise being equivalent to a noiseless detector with a reduced quantum efficiency given by the detective quantum efficiency (DQE) defined as[10] $\text{DQE}=(\text{S/N})_o^2/(\text{S/N})_i^2$, the square of the signal to noise ratio of the output divided by that of the input signal. The total noise in the output signal is composed of photoelectric shot noise and readout noise, $\sigma_{\text{total}}^2=\sigma_{\text{shot}}^2+\sigma_{\text{readout}}^2$, while that of the input is simply the shot noise of the input photon flux.

In the case of the CCD detector, there is a contribution to the noise in the detected signal from the readout electronics, therefore the DQE can be written:

$$\text{DQE}_{\text{CCD}}=\frac{(I\eta)^2/(I\eta+r^2)}{(I/\sqrt{I})^2}=\frac{\eta^2 I}{\eta I+r^2}, \tag{5}$$

where I is the input flux, η the photodetector quantum efficiency and r the readout noise (equivalent to 6.7 electrons). At a typical signal level of $I\eta=50$ p-e $\text{pix}^{-1}\,\text{scan}^{-1}$ and with a quantum efficiency η of 0.8, the DQE is 0.422, roughly half the value for a noiseless detector.

For the MCP detector the readout noise of the diode array is small compared to the intensity of the light output from the image intensifier. However the image intensification process itself introduces an effective noise due to the statistical nature of the electron amplification process in the channel plates. From photomultiplier theory[11] the noise in the output signal may be written

$$\sigma^2=\eta I f g^2 \tag{6}$$

where g is the gain of the tube and f is a factor between 1 and 2 dependent on the secondary emission characteristic of the multiplier. This leads to an expression for the DQE of the MCP detector:

$$\text{DQE}_{\text{MCP}}=\frac{(gI\eta)^2/(I\eta f g^2+r^2)}{(I/\sqrt{I})^2}=\frac{\eta}{f+r^2/I\eta g^2}. \tag{7}$$

In the case that the readout noise is small compared to the signal, this expression reduces to η/f. For a MCP operating in current mode, with a nonsaturated output pulse, the value of f is probably close to 2, leading to a DQE equal to half the primary quantum efficiency.

The above analyses therefore result in DQEs for the two detectors that are both about half the primary photoconversion efficiencies, which, taken with the calculated $\sqrt{A}$ dependence of the uncertainty in the fitted position, yields the result that this uncertainty should depend upon the square root of the ratio of the primary quantum efficiencies, as observed in practice (Fig. 9).

Using the expressions for the DQE of the CCD detector [Eq. (5)] and the equivalent expression for the MCP detector [including the readout noise at the measured level of 1 count rms, Eq. (7)] the position uncertainties can be plotted for each detector as a function of illumination. These curves, shown in Fig. 8, are close to the inverse square root form over the range of illuminations used in the measurements and as seen in the experimental data. The absolute values of the uncertainties depend on implicit assumptions about the linewidth and so the model curves differ from the experimental data by an arbitrary factor (although the same factor for each model curve).

The approximate square root dependence of the σ on countrate is seen in the linear slopes of Figs. 6 and 8 over more than an order of magnitude variation in count rate. The CCD has a lower σ for both the fitted width and position parameters by a factor of 2.25. This ratio is close to the square root of the ratio by which the quantum efficiency of the CCD detector exceeds that of the MCP detector at 530 nm; $\sqrt{\nu_{\mathrm{CCD}}/\nu_{\mathrm{MCP}}}=\sqrt{0.60/0.07}=2.93$. The variation of this ratio with wavelength shown in Fig. 9 closely follows the variation of quantum efficiency and provides confirmation that it is the photoelectron rate that determines the σ.

From the analysis of the tokamak data it is found that the apparent sensitivity of the CCD detector is greater by a factor of 13.7 than that of the MCP, assuming equal emission from the plasma in the two shots. The ratio of the QEs of the two detectors is only 8.6, indicating an extra factor 1.6 gain of the CCD system over the MCP detector. In part this is certainly due to the image of the entrance slits of the spectrometer being vertically extended at the exit by the astigmatism of the instrument. Since the entrance slits are exactly the same height (2.5 mm) as the MCP detector pixels there is inevitably some light loss in this system, whereas the CCD binned pixels (288 pixels—6.3 mm—high in this case) are certain to collect all the light. Furthermore, the MCP system will be sensitive to any misalignment between the output image and the detector.

Equation (4) shows no simple dependence of the variance in fitted position with the spectral linewidth. While the lamp measurements in Sec. III D show evidence of a $(\mathrm{width})^{3/2}$ dependence. The ratios of the variances of the two detectors in the tokamak measurements follow the square root dependence on signal intensity, but the absolute value of the separate variances derived from Eq. (1) are approximately twice those measured in the tokamak data. An exponent of 1/3 on the width in Eq. (1) recovers agreement between the laboratory data of Fig. 8 and the tokamak measurements. Potentially the disagreement arises from the deviation from Gaussian of the defocused line image used in the laboratory measurements, however expressing the width dependence as a simple power law is clearly an oversimplification.

The weak dependence of the σ values on V_{pc}, as seen in Fig. 7 above 1400 V, despite the factor 50 change in electron gain, is further evidence that the $\sigma_{\mathrm{position}}$ depends on the number of detected photons (i.e., on the QE) not on the details of the later amplification and digitization processes. At the lowest voltages the sensitivity of the detector is about 10 photoelectrons per ADC count whereas at normal operating voltages it is close to one. This shows that the signal to noise ratio in the detected signal is not the relevant factor, at least in the operating regime explored.

ACKNOWLEDGMENTS

This work was funded by the UK Department of Trade and Industry and Euratom. Part of the work was performed under a collaborative agreement between Culham Laboratory and the JET Joint Undertaking.

[1] J. C. Twichell, B. E. Burke, R. K. Reich, W. H. McGonagle, C. M. Huang, M. W. Bautz, J. P. Doty, G. R. Ricker, R. W. Mountain, and V. S. Dolat, Rev. Sci. Instrum. **61**, 2744 (1990).
[2] N. Hawkes, in *Proceedings of the 20*th *European Conference on Controlled Fusion and Plasma Physics* (European Physical Society, Petit-Lancy, Switzerland, 1993), Vol. II, p. 3.
[3] N. Hawkes and N. Peacock, Rev. Sci. Instrum. **63**, 5164 (1992).
[4] Photek model MCP 240 EG. Photek, 26, Castleham Road, St Leonards-on-Sea, East Sussex, TN38 9NS, UK.
[5] J. S. Haskovec, G. Bramson, N. H. Brooks, and M. Perry, General Atomics Report GA-A 19753, December 1989.
[6] Wright Instruments, Unit 10, 26 Queensway, Enfield, Middlesex, EN3 4SA, UK.
[7] W. H. Press, B. P. Flannery, S. A. Teukolsky, and W. T. Vetterling, *Numerical Recipies*, 1st ed. (Cambridge University Press, Cambridge, 1986).
[8] N. C. Hawkes and N. J. Peacock, Rev. Sci. Instrum. **63**, 5164 (1992).
[9] A. B Anton, Rev. Sci. Instrum. **62**, 832 (1991).
[10] S. S. Vogt, R. G. Tull, and P. Kelton, Rev. Sci. Instrum. **17**, 574 (1978).
[11] Statistical Theory of Noise in Photomultiplier Tubes, Photomultiplier Handbook (Burle Industries Inc., Tube Products Division, 1000 New Holland Ave., Lancaster, PA 17601-5688), Appendix G.